American Mineralogist, Volume 103, pages 1770–1779, 2018

Liquid properties in the Fe-FeS system under moderate pressure: Tool box to model small planetary cores

Guillaume Morard[1,*], Johann Bouchet[2], Attilio Rivoldini[3], Daniele Antonangeli[1], Mathilde Roberge[1], Eglantine Boulard[1], Adrien Denoeud[4], and Mohamed Mezouar[5]

[1]Sorbonne Université, Muséum National d'Histoire Naturelle, UMR CNRS 7590, IRD, Institut de Minéralogie, de Physique des Matériaux et de Cosmochimie, IMPMC, 75005 Paris, France
[2]CEA, DAM, 91297 Arpajon, France
[3]Royal Observatory of Belgium, B-1180 Bruxelles Belgium
[4]Ecole Polytechnique, LULI, F-91128 Palaiseau, France
[5]European Synchrotron Radiation Facility, Grenoble F-38043 France

Abstract

Physical properties of liquid Fe-S alloys (from 10 to 50 at%S) under high pressure were investigated by in situ X-ray diffraction (up to 5 GPa and 1900 K) and by ab initio calculations. The local structure of Fe-S liquid alloys clearly shows how S modifies the local arrangement of the Fe atoms. Density has been extracted from the diffuse scattering by minimization of the oscillation in the short distance of the radial distribution function $g(r)$. Two different formalisms for the *P-V-T-X* equation of state are presented to model density and sound velocity as a function of pressure, temperature, and sulfur content. Based on these results, Moon's core composition is discussed. This coherent data set will serve as a thermodynamically consistent ground for modeling the core of small telluric planets and large icy satellites.

Keywords: Iron alloys, liquid, Fe-S liquid, planetary cores

Introduction

Elements lighter than iron are expected to be present in planetary cores, due to their abundance in iron meteorites and their affinity with the metallic phase. Among the potential light elements (Poirier 1994), sulfur is likely the most abundant in the cores of iron meteorites parent bodies (Chabot 2004). From tungsten isotopes data (Kleine et al. 2009) and experimental studies of percolation processes (Yoshino et al. 2003), core formation is expected to occur within a few million years of the solar system formation, even in small planetesimals (Greenwood et al. 2006). It is therefore important to constrain the physical properties of Fe-S liquid alloys to better understand core formation in the early stage of the solar system.

Melting properties in the Fe-FeS system under high pressure have been intensively investigated by in situ (Campbell et al. 2007; Morard et al. 2007b, 2008a, 2008b; Chen et al. 2008a; Andrault et al. 2009) or ex-situ methods (Chudinovskikh and Boehler 2007; Stewart et al. 2007; Chen et al. 2008b; Kamada et al. 2012). However, although the Fe-rich side of the phase diagram begins to be relatively well described, we still lack precise knowledge of important physical properties, especially in the liquid state such as density or viscosity (LeBlanc and Secco 1996; Sanloup et al. 2000; Vočadlo et al. 2000; Balog et al. 2003; Nishida et al. 2008).

As today, the inner structures and in particular the cores of planetary bodies in the solar system are not well known, mostly because of the absence of seismological data, with the clear exception for the Earth and, to some extent, for the Moon. Inferences about planetary cores can be obtained from geodesy, electrical, and magnetic data and size, density, and composition have been estimated (e.g., Yoder et al. 2003; Margot et al. 2007; Rivoldini et al. 2009; Zhang and Pommier 2017). However, those inferences require detailed modeling of the interior structure, and the precision of the estimates, in particular core composition, calls for extensive knowledge about core material properties. In this study, we investigated the density of liquid Fe-S alloys up to 5 GPa and 1900 K and assessed how it affects the lunar interior.

Simultaneous measurements of density and liquid structure have been performed to emphasize the strong link between the evolution of the local atomic arrangement and changes in the liquid density. This experimental study has been complemented by ab initio calculations of the liquid structure in similar *P-T* conditions. We present two models describing thermoelastic properties of liquid Fe-S as a function of pressure, temperature, and S content based on our data and results published in the literature. These models are finally applied to estimate S content in Moon's core.

Experimental procedures

Paris-Edinburgh Press experiments

X-ray diffraction experiments were carried out at the High Pressure Beamline ID27 at ESRF in Grenoble, France (Mezouar et al. 2005) using a large volume VX5 type Paris-Edinburgh Press (PEP) (Besson et al. 1992; Klotz et al. 2005). This press allows large opening angle in the equatorial plane. The very high brilliance X-ray beam delivered by two in-vacuum undulators was collimated down to 50×50 μm (typical values). The X-ray wavelength was fixed to $\lambda = 0.24678$ Å (gadolinium *K*-edge) using a Si(111) channel-cut monochromator. A multichannel collimator (Mezouar et al. 2002; Morard et al. 2011) was used to minimize the X-ray background coming from sample environment materials. The data were collected using a MAR345 imaging plate system (X-ray research company GmbH,

* E-mail: guillaume.morard@impmc.upmc.fr

0003-004X/18/0011–1770$05.00/DOI: https://doi.org/10.2138/am-2018-6405

Norderstedt, Germany). The sample-detector distance was calibrated with a LaB_6 standard powder and the diffraction images were treated and integrated using the Fit2D software (Hammersley et al. 1996). Typical exposure time to obtain the hereby presented data is 300 s.

The high-pressure chamber consists of two opposed tungsten carbide anvils that have quasi-conical hollows. We used 7 mm boron epoxy gaskets with a classical cell assembly [graphite cylinder furnace, MgO capsule used as pressure medium and electrical insulator (Mezouar et al. 1999)]. MgO polycrystalline capsule is softer than single-crystal alumina capsule, used for conventional X-ray radiography technique, so to minimize pressure gradients in the cell (Nishida et al. 2016). The pressure was calibrated using the equation of state (EoS) of MgO (Utsumi et al. 1998) close to the sample, to reduce *P-T* uncertainties. The temperature was fitted using a previously established calibration curve (Morard et al. 2007a). By the combined use of this calibration and MgO EoS, the pressure was found to be stable up to 1570 K and to decrease at higher temperatures (up to 0.7 GPa for the highest temperature). With increasing temperature, we could track the structural transitions in Fe (Klotz et al. 2008) and FeS (Urakawa et al. 2004), confirming the validity of the temperature calibration. As addressed in details in a previous paper (Morard et al. 2007b), metrological uncertainties are the following: 170 K in temperature and 0.6 GPa in pressure.

The samples were a mixture of pure Fe (99.99%, Alfa Aesar) and FeS powders (99.9%, Sigma Aldrich). Electron microprobe (EMP) analyses were performed on quenched samples (Centre Camparis, UPMC, Paris) using a Cameca SX100 wavelength-dispersive spectrometer (WDS) to measure the three main elements in this study (Fe, S, and O, as a potential pollutant). Operating conditions in both cases were 15 kV and 40 nA for a counting time of 20 s at peak and 10 s at the background. Standards for the three elements were Fe, FeS_2, and Fe_2O_3, respectively. Our samples show fine dendritic textures; therefore we used a defocused beam of ~20 µm to average the compositions of quenched texture (Fig. 1).

Density and liquid structure of liquid Fe-S alloys were extracted from the diffuse scattering signal recorded under high pressure and high temperature. A diffuse signal with high quality was recorded on a Q range up to almost 100 nm^{-1}, allowing measurements up to the third oscillation of the structure factor S(Q) (Fig. 2). Analysis of angle dispersive liquid diffuse signal recorded using PEP is detailed in a previous paper (Morard et al. 2013). Uncertainties on experimentally measured density values of ±3 atoms/nm^3 (equivalent to ~250 kg/m^3) were estimated from Q range, self-absorption and minimal distance on the radial distribution function $g(r)$ (Table 1) (Morard et al. 2013).

Molecular dynamics calculations

Simulations were performed using the ABINIT package (Gonze et al. 2016). The electrons are treated quantum mechanically using density functional theory (DFT) while the movement of the ions is treated classically using the resulting forces. The calculations used the projected augmented wave (PAW) (Blochl 1994; Torrent et al. 2008) method for the computation of the electronic structure and the generalized gradient approximation (GGA) following the parametrization of Perdew, Burke, and Ernzerhof (PBE) for the exchange-correlation energy and potential (Perdew et al. 1996). For iron, we generated a pseudo-potential with 3*s*, 3*p*, 3*d*, and 4*s* states as valence electrons (see (Dewaele et al. 2008; Bouchet et al. 2013) for a detailed description of the generation of the pseudopotential and a comparison with recent experimental data). For sulfur, the pseudo-potential includes 3*s* and 3*p* states as valence electrons. The simulations were performed using a cutoff energy, E_c, for the plane wave basis chosen equal to 350 eV. The radius of the augmentation regions for the PAW pseudo-potential was chosen small enough to avoid an overlapping of the spheres surrounding each atom at the highest densities. An efficient scheme for the parallelization present in ABINIT was used to perform the simulations involving a large number of atoms and time steps (Bottin et al. 2008).

We used supercells of liquid Fe of 128 atoms and we replace 13, 17, 29, 38, 50, and 64 atoms of Fe by atoms of S to obtain a composition of 10 at% S, 23 at% S, 30 at% S, 39 at% S, and 50 at% S, respectively. The simulations were first performed in the NPT (constant number of atoms, pressure, and temperature) ensemble to reach the desired pressure (5 GPa) and then in the NVT (constant number of atoms, volume, and temperature) ensemble to avoid any fluctuations of cell parameters. The temperature was fixed to 2500 K and we systematically used an electronic temperature

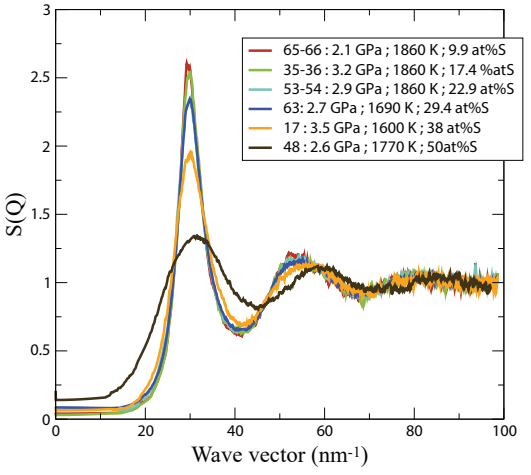

FIGURE 2. Structure factors S(Q) of liquid Fe-S alloys as a function of the composition for similar *P-T* conditions. (Color online.)

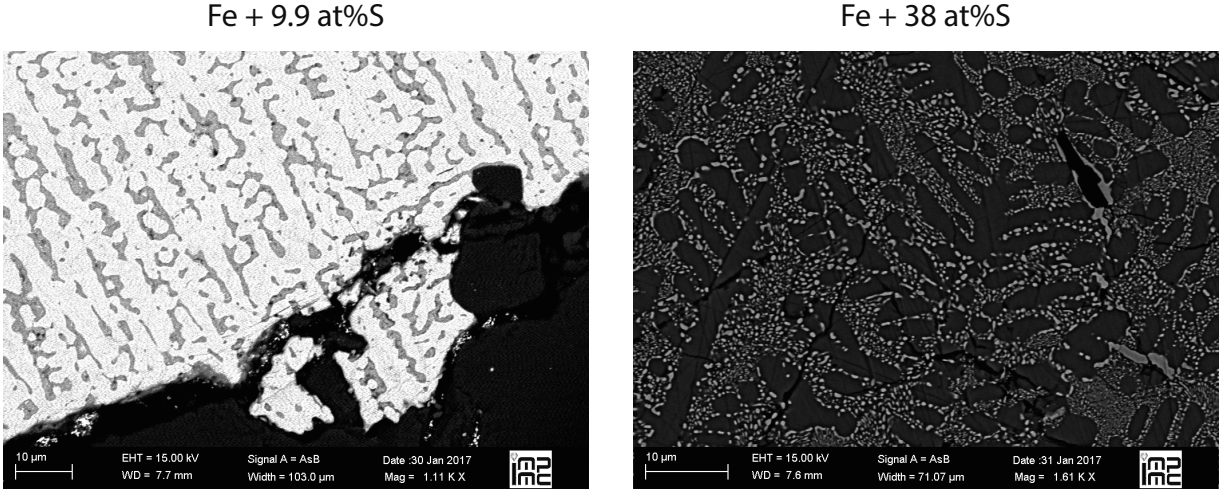

FIGURE 1. Scanning electron microscope (SEM) images of polished cross sections of recovered samples. Here are presented two different compositions, with typical quench textures of S-poor and S-rich liquids. Microprobe measurements were performed on a large area, ~20 µm, to average the composition over these textures.

equal to the ionic temperature in our simulations. This relatively high temperature is necessary to ensure the complete melting of the supercells.

Once the box of simulated atoms is equilibrated (after at least 5 ps), partial radial distributions functions, $g(r)$, for Fe–Fe, Fe–S and S–S atoms were calculated from 2.5 ps time averages taken different starting times to ensure the convergence. It is well known that at room pressure the experimental equilibrium volume of iron is underestimated in DFT-GGA-PBE calculations due to an incorrect modeling of magnetic effects (Dewaele et al. 2008) by around 7% and therefore the density is overestimated by the same percentage. The bulk modulus is also strongly overestimated (Dewaele et al. 2008), and therefore the density discrepancies between DFT_GGA and experiments hold up to high pressure (around 150 GPa). Note that it is possible to correct the GGA results by using the dynamical mean-field theory (Pourovskii et al. 2013) and to recover a good agreement with the experimental equation of state, but this approximation cannot be used in molecular dynamics calculations due to its enormous computational cost. For solid Fe-S in the B2 structure, the density overestimation is similar (Sherman 1995). We reproduce these discrepancies in our calculations for liquid Fe-S with a constant overestimation of the experimental density by about 1000 kg/m^3, due to the GGA-PBE, but also to a larger pressure in the calculations. Noteworthy, the overall evolution of the density as a function of the sulfur composition is comparable to that experimentally measured.

Results and Discussion

Liquid structure

Analysis by Fourier transform of the diffuse X-ray scattering of liquid metals gives access to the local structure $g(r)$ of the liquid (Fig. 3). In addition to the experimental results, ab initio calculations have been performed on this system in a similar P-T range. As already mentioned, inherent problems of calculations involving iron, without modeling magnetic properties correctly, leads to a known overestimation of the density. However, the main features of experimental and theoretical liquid structures are relatively similar. It should be noticed that oscillations present in the experimental data of the structure of pure FeS liquid are not real but are related to the spurious signal coming from limited Q range on the corresponding structure factor.

Irrespectively of the density shift, simulations bring additional information impossible to obtain with the present XRD experiments: partial $g(r)$ have been be extracted from the calculations (Fig. 4), showing no S-S polymerization on the Fe-FeS side of the phase diagram, in agreement with previous published calculations using smaller supercells (64 atoms compared to 128 in our MD simulations) (Alfè and Gillan 1998; Vočadlo et al. 2000). The S-S bond remains large, emphasizing S-S repulsion, and no formation of S-S clusters for all studied compositions. This definitely rules out the idea that S-S interactions were at the origin of the anomalous values of the viscosity (LeBlanc and Secco 1996).

Partial $g(r)$ does not show any drastic change in the bond lengths with increasing S content (Fig. 4). The Fe-S bond is

Table 1. Pressure-temperature conditions, chemical composition of quenched samples, and densities measured and calculated at 1900 K

Run number	P (GPa)	T (K)	x_S (at%)	Density (atoms/nm^3)	Density (kg/m^3)	Density at 1900 K (kg/m^3)	CN1	CN2	r1 (nm)
31-32	4.2 ± 0.6	1900 ± 170	9.9	76.9 ± 3	6830 ± 270	6830 ± 270	8.05	9.26	2564
34-35	4.1 ± 0.6	1980 ± 170	9.9	76.1 ± 3	6760 ± 270	6840 ± 270	7.94	9.12	2567
61-62	2.2 ± 0.6	1780 ± 170	9.9	75.8 ± 3	6730 ± 270	6630 ± 270	7.97	9.18	2578
65-66	2.1 ± 0.6	1860 ± 170	9.9	75 ± 3	6660 ± 270	6630 ± 270	7.85	9.05	2581
35-36	3.2 ± 0.6	1860 ± 170	17.4	76.4 ± 3	6560 ± 260	6520 ± 260	7.88	9.14	2569
49-50	2.9 ± 0.6	1780 ± 170	22.9	74 ± 3	6190 ± 250	6090 ± 250	7.64	8.88	2571
53-54	2.9 ± 0.6	1860 ± 170	22.9	73.4 ± 3	6140 ± 250	6110 ± 250	7.54	8.75	2572
89-90	1.7 ± 0.6	1780 ± 170	22.9	70.4 ± 3	5890 ± 250	5790 ± 250	7.32	8.45	2.59
91-92	1.5 ± 0.6	1860 ± 170	22.9	70 ± 3	5860 ± 250	5830 ± 250	7.26	8.4	2589
42	5 ± 0.6	1750 ± 170	29.4	75.2 ± 3	6100 ± 240	5980 ± 240	7.71	8.95	2552
63	2.7 ± 0.6	1690 ± 170	29.4	72.2 ± 3	5860 ± 240	5690 ± 240	7.43	8.61	2566
17	3.5 ± 0.6	1600 ± 170	38	71.9 ± 3	5590 ± 230	5370 ± 230	6.86	8	2543
25	5.2 ± 0.6	1870 ± 170	50	59.8 ± 3	4360 ± 220	4340 ± 220	3.96	4.5	2415
48	2.6 ± 0.6	1770 ± 170	50	57.3 ± 3	4180 ± 220	4100 ± 220	3.77	4.28	2423

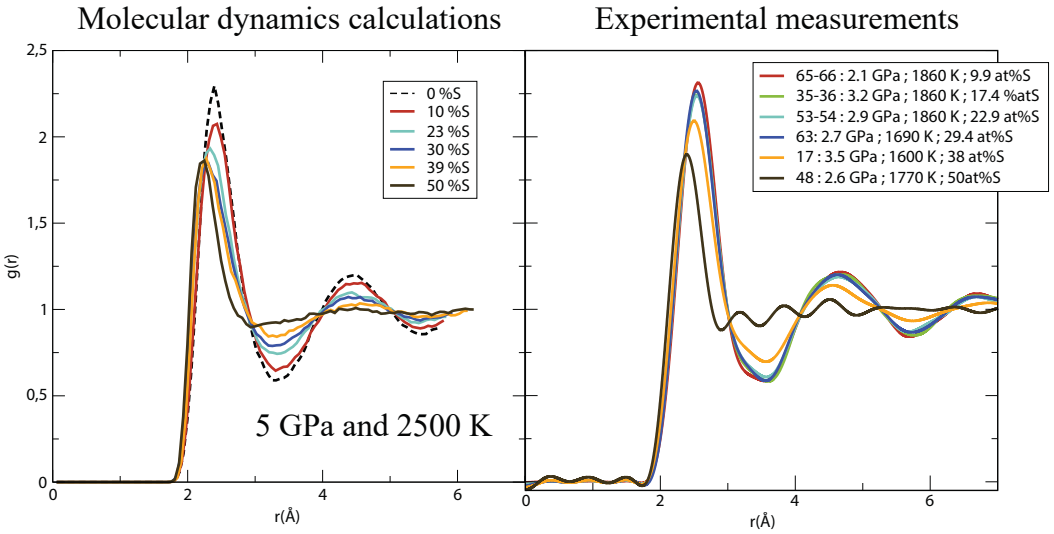

Figure 3. Comparison between pair distribution function $g(r)$ obtained from ab initio calculations (5 GPa and 2500 K) and experimental results (similar P-T conditions and composition as in Fig. 2). (Color online.)

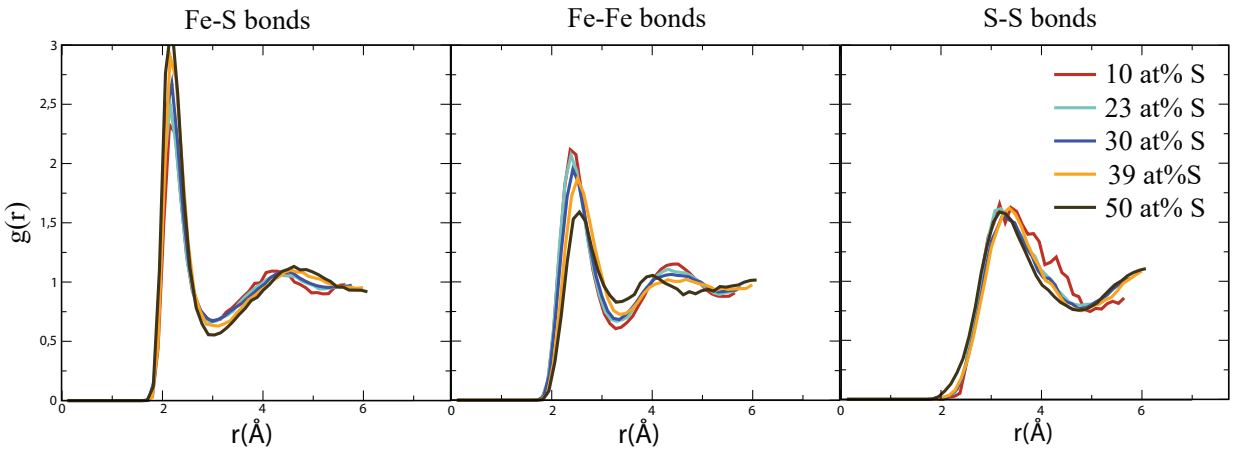

FIGURE 4. Partial pair distribution function for different composition extracted from the ab initio calculations. (Color online.)

shorter than the Fe-Fe bond, this is related to the covalent status of this bond (Flory et al. 2005; Morard et al. 2008a, 2008b). The position of the first peak in the $g(r)$, directly related to the first coordinance sphere (CS), was observed in the experiments to remain relatively unchanged up to ~30 at% S and to drastically decrease for larger sulfur concentrations (Fig. 5). As the contribution of each X-X atomic pair to the total $g(r)$ probed by X-ray is related to the weight of the atoms, the first peak position is essentially associated with the Fe-Fe network. S-S bond is relatively longer (3.4 Å) but with lower intensity and larger dispersion, whereas Fe-S bonds are shorter (2.2 Å) than Fe-Fe bonds (2.5 Å) and have a higher intensity. It is, therefore, the addition of Fe-S bonds that influenced the total $g(r)$ observed in our experiments and explained the shortening of the observed first CS position (Fig. 5). The hereby presented peak position is in relatively good agreement with previous results from (Kono et al. 2015).

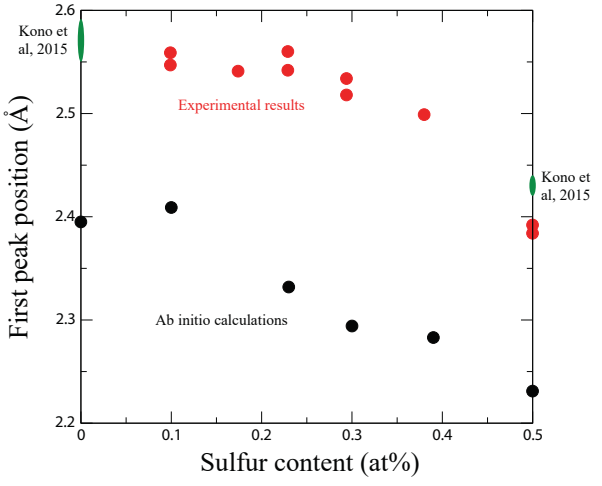

FIGURE 5. First peak position as a function of the S content for the different $g(r)$, compared with theoretical work, and previous results from (Kono et al. 2015). (Color online.)

Comparison of our data set with the literature

The Fe-FeS binary system has been studied extensively over a large pressure range. The density of liquid Fe-S alloys has been determined by ex-situ sink-float method (Balog et al. 2003; Nishida et al. 2008), by in situ X-ray radiography (J. Chen et al. 2014), and by X-ray absorption (Sanloup et al. 2000; Nishida et al. 2011). These data sets do not provide a consistent picture, and the derived densities show large discrepancies, even when measurements have been performed with the same method. Sound velocities of liquid Fe-S alloys have been probed in situ under high pressure by conventional ultrasonic method but, as for the density measurements, the results by different research groups are in disagreement (Nishida et al. 2013, 2016; Jing et al. 2014). A thorough comparison of our new measurements (Table 1) with literature results will shed light on the properties of the Fe-S binary system at high pressure and high temperature.

Regarding pure liquid FeS, previous studies have found contradictory results (Nishida et al. 2011; B. Chen et al. 2014) in spite of using the same X-ray absorption technique. Chen et al. argue that the reported density difference can be explained by the temperature difference. Specifically, they claim that the temperature difference of 150 K can account for a density difference of almost 400 kg/m^3. However, such a large thermal expansion is incompatible with ambient pressure measurements [for pure FeS, the liquid density only changes from ~3900 to ~3820 kg/m^3 between 1473 and 1623 K (Kaiura and Toguri 1979)]. Furthermore, a combined fit of either of the two high-pressure sets of density for pure liquid FeS with ambient-pressure results is impossible using conventional EoS values and requires an unrealistically small K_{T0} (Nishida et al. 2011). Conversely, the here-measured density for pure liquid FeS at high pressure are in good agreement with ambient pressure measurements (Nagamori 1969; Kaiura and Toguri 1979), while differ from the previous high-pressure measurements (the difference between the present data set at 4 GPa and 1900 K and previous determination is 6% (Nishida et al. 2008), 10% (Nishida et al. 2011), and 20% (J. Chen et al. 2014) (Fig. 6).

Unlike liquid density measurements at high pressure, literature concerning measurements on liquid Fe-S alloys at ambient pressure is limited and relatively old (Nagamori 1969; Kaiura and Toguri 1979). It should also be noted that there are no density

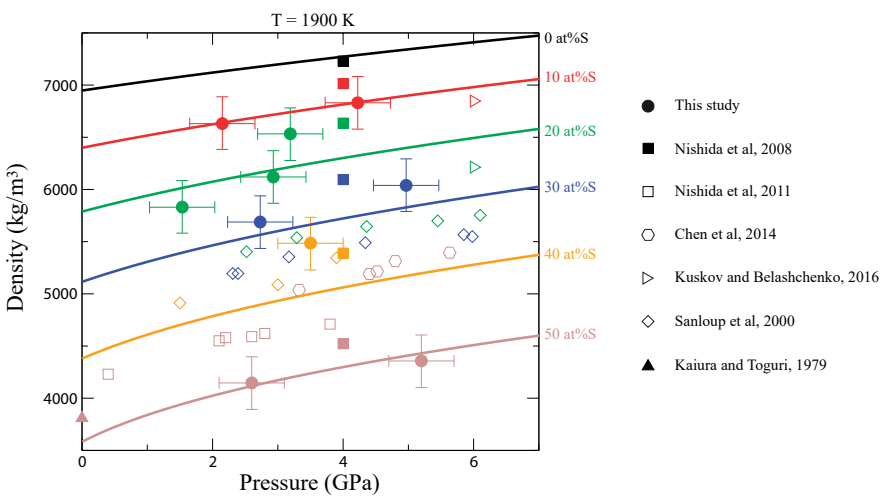

FIGURE 6. The density of liquid iron alloys from this study and the corresponding thermodynamic model compared with available measurements. The color of the different symbol is related to the composition, rounded to the closest nominal value. (Color online.)

measurements over a wide compositional range (0–40 at% S) at ambient pressure. Regarding pure liquid Fe, measurements have been recently performed over a wide temperature range, allowing a very good estimation of the density/temperature relation (Assael et al. 2006), which is used to extract density of liquid Fe-S alloys at 1900 K as a function of S content (Fig. 7).

The density of the liquid Fe-S alloys at ambient pressure (ρ_0) is a sensitive parameter in our study. Drastically different models have been used in previous studies (Fig. 7), with a deviation of ~1000 kg/m³ for close compositions in the 15–20 at% S range. We anchor our study on ambient-pressure measurements, fixing the density for the 40–50 at% S alloys on those by Nagamori (1969) extrapolated at 1900 K using thermal expansion from Kaiura and Toguri (1979). A quadratic polynomial fit is then performed to interpolate between the density of S-rich alloys and that of pure liquid Fe, fixed to the value of Assael et al. (2006). This trend is in relatively good agreement with densities calculated by ab initio techniques (Kuskov and Belashchenko 2016) for low S concentration (Fig. 7). The so-derived second-order polynomial gives:

$$\rho = -3108X_S^2 - 5176X_S + 6950 \quad (1)$$

where X_S is the S concentration in atom%. Looking at this relation, it comes clearly out that values of density from Sanloup et al. (2000) and the related model from Jing et al. (2014) are too low, in particular for low S content, and in disagreement with our model (Fig. 7).

Regarding sound velocity, most recent measurements (Nishida et al. 2016) and calculations (Kuskov and Belashchenko 2016) are incompatible with ambient-pressure measurements (Nasch et al. 1997; Nasch and Manghnani 1998) (Figs. 8 and 9), while previous measurements on Fe-16at%S are (Jing et al. 2014) (Fig. 9). Our model is therefore adjusted to agree with Jing et al. (2014).

To conclude, a survey of the literature on Fe-S liquid alloys under high pressure show relatively scattered results. Strong disagreement exists for density, sound velocity, and thermal expansion. Our approach is to anchor our model on ambient-pressure measurements, with only a few assumptions, as for example the interpolation of liquid density between 0 and 40 at% S.

Parametrized equation of state

To fit our set of density data, we use a third-order Birch Murnaghan equation of state relating pressure P and density ρ at the fixed temperature of 1900 K:

$$P = \frac{3}{2}K_{T0}\left[\left(\frac{\rho}{\rho_0}\right)^{7/3} - \left(\frac{\rho}{\rho_0}\right)^{5/3}\right]\left[1+\frac{3}{4}(K_0'-4)\right]\left[\left(\frac{\rho}{\rho_0}\right)^{2/3}\right] - 1 \quad (2)$$

where K_{T0} is the isothermal bulk modulus at ambient pressure and 1900 K, K' is the pressure derivative of the bulk modulus and ρ_0 is the density at ambient pressure and 1900 K. Each parameter is a function of molar S content in the liquid (X_S). The isothermal bulk modulus at ambient pressure and its derivative can be expressed as follows (J. Chen et al. 2014):

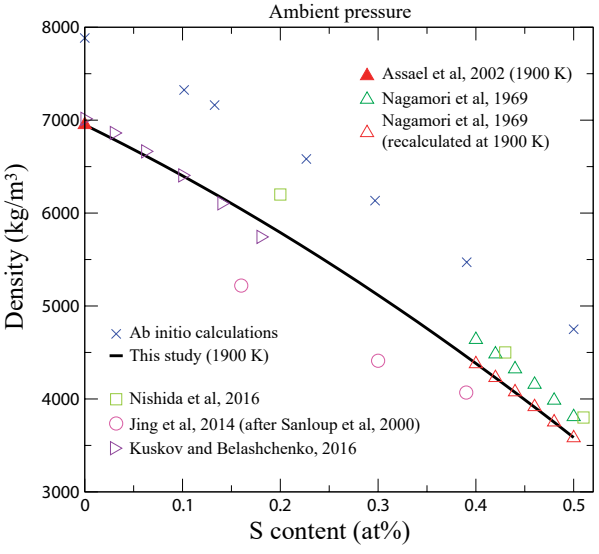

FIGURE 7. The density of liquid Fe-S alloys at ambient pressure from different studies. Our thermodynamic model uses an interpolation between the density of pure Fe from Assael et al. (2006) and densities of S-rich liquids (Nagamori 1969) corrected for temperature difference following Kaiura and Toguri (1979). (Color online.)

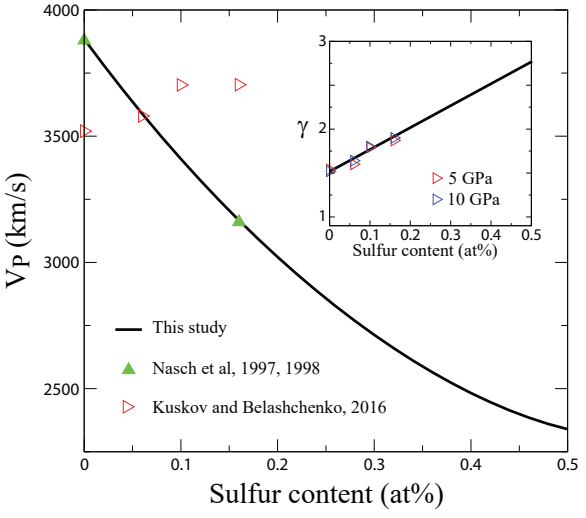

FIGURE 8. Sound velocity fit for this model as a function of S content based on measurements at ambient pressure from Nasch et al. (1997) and Nasch and Manghnani (1998), compared with theoretical calculations from Kuskov and Belashchenko (2016). Inset: Gruneisen parameter used in this model compared with ab initio calculations from Kuskov and Belashchenko (2016). (Color online.)

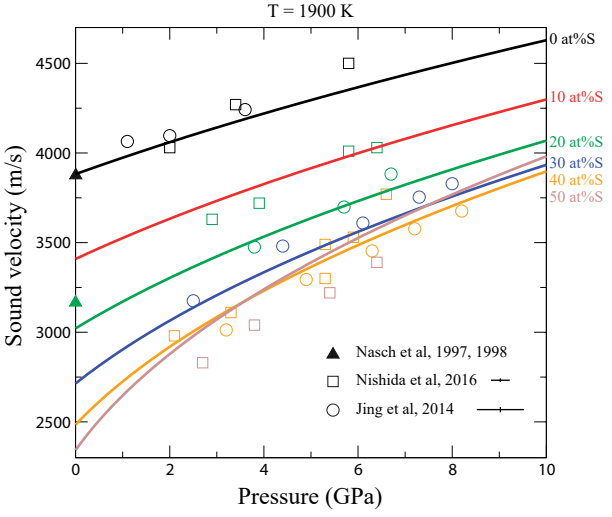

FIGURE 9. Sound velocity extracted from our thermodynamic model compared to the available literature (Nasch et al. 1997; Nasch and Manghnani 1998; Jing et al. 2014; Nishida et al. 2016). Different colors correspond to different compositions, rounded to the closest nominal value. Representative error bars for the two high-pressure studies have been added in the figure legend. (Color online.)

$$K_{T0} = K_{T,Fe}^{1-X_S} \times K_{T,S}^{X_S}. \quad (3)$$

A linear mixing law for bulk moduli could be used, but for a shorter range of composition (Morard et al. 2013). In the present study, we found more suitable to use such type of mixing law. More details regarding different mixing law for bulk moduli can be found in Chen et al. 2014.

For pure Fe we assume K_T,Fe = 76 GPa. This value is deduced from sound velocity measurements at 1 bar (Nasch and Manghnani 1998), assuming a value for the specific heat at constant volume C_V of 4R and the value of specific heat at constant pressure C_P as in (Nasch and Steinemann 1995). Regarding sulfur, we take K_T,S = 1.6 GPa (Tsuchiya 1994) as in Chen et al. (2014), which gives an overall good agreement with compressibility data from Nishida et al. (2011). However, it should be noticed that this value is measured at 673 K and not at 1900 K. Accordingly, this parameter should be considered a fitting parameter, restraining the validity of our model only between Fe and FeS compounds.

As measurements in the 0–5 GPa range do not cover a large enough pressure range to adequately constrain K' values, this is adjusted to fit the velocity measurements, following the relation $K' = K'_{Fe} + X_S \cdot 3$, with $K'_{Fe} = 6.5$.

As our measurements were performed at different temperatures, we also need to estimate thermal expansion as a function of pressure, temperature, and S content. We assume a linear dependence of density on temperature [experimentally proven for liquid iron (Assael et al. 2006)]. We calculate the thermal expansion at 1900 K, assuming linearity between Fe and FeS:

$$\alpha_0 = -\frac{1}{\rho_0}\left(\frac{\partial \rho}{\partial T}\right)_0 \quad (4)$$

$$\left(\frac{\partial \rho}{\partial T}\right)_{Fe,0} = 0.926 \quad \text{from (Assael et al. 2006)}$$

$$\left(\frac{\partial \rho}{\partial T}\right)_{FeS,0} = 0.533 \quad \text{from (Kaiura and Toguri 1979)}$$

$$\left(\frac{\partial \rho}{\partial T}\right)_0 = \left(\frac{\partial \rho}{\partial T}\right)_{Fe,0} - 2\left(\left(\frac{\partial \rho}{\partial T}\right)_{Fe,0} - \left(\frac{\partial \rho}{\partial T}\right)_{FeS,0}\right) X_S. \quad (5)$$

Due to the lack of data on thermal expansion for intermediate compositions, we chose a linear mixing for the thermal expansion mixing model. More detailed investigation is required in the future to better constrain this linear model.

Then, thermal expansion at a given pressure is calculated under the assumption:

$$\alpha_0 K_{T,0} = \alpha K_T \quad (6)$$

with

$$K_T = \frac{K_{T0}}{2}\left[7\left(\frac{\rho}{\rho_0}\right)^{7/3} - 5\left(\frac{\rho}{\rho_0}\right)^{5/3}\right]\left[1 + \frac{3}{4}(K'_0 - 4)\left(\left(\frac{\rho}{\rho_0}\right)^{2/3} - 1\right)\right] + \frac{3K_{T0}}{4}\left[(K'_0 - 4)\left(\left(\frac{\rho}{\rho_0}\right)^3 - \left(\frac{\rho}{\rho_0}\right)^{7/3}\right)\right]. \quad (7)$$

A parameter that could be directly derived from our EoS is the compressional sound velocity in the liquid:

$$V_P = \sqrt{\frac{K_T(1 + \alpha\gamma T)}{\rho}}. \quad (8)$$

The value of the Grüneisen parameter of the liquid Fe-S alloy is calculated from the V_P of pure Fe and Fe-16 at% . S (Nasch et al. 1997; Nasch and Manghnani 1998) (Fig. 8, inset) assuming that the Grüneisen parameter evolves linearly with the sulfur concentration. The values obtained are in agreement with ab initio calculations in Kuskov and Belashchenko (2016) (Fig. 8, inset). However, calculations from (Kuskov and Belashchenko 2016) argue for an increase of the sound velocity as a function of S content, whereas experimental data show the opposite behavior (Fig. 8). In addition, Grüneisen parameter is assumed to be constant in the pressure range 0–10 GPa. This seems reasonable over a relatively small pressure range (Kuskov and Belashchenko 2016). The Grüneisen parameter varies here as $\gamma = 1.52+2.5X_S$.

Thermodynamic model

In addition to the empirical parametrization introduced above, we also provide a description of the thermoelastic properties of liquid Fe-S alloys based on thermodynamic solution modeling. This approach is complementary to the previous one and is based on the mixing of the end-members: pure liquid Fe and FeS. For liquid Fe we use the EoS of Komabayashi (2014) and for liquid FeS, an EoS deduced from our density data and from sound velocity data of Nishida et al. (2016). For both end-members we use a Vinet equation for isothermal compression and an Anderson-Grüneisen parametrization for isobaric heating (see Komabayashi 2014). The parameters for liquid FeS EoS are given in Table 2. To assess the solution model that best describes our density data and the sound velocity data of Nishida et al. (2016) over the entire Fe-FeS binary, we test three different mixing models that affect the volume of the solution, assuming (1) ideality; (2) concentration-dependent non-ideality; and (3) concentration and pressure dependent non-ideality.

To model the excess contribution we use the Margules parameterization, introduced by Buono and Walker (2011), to describe the non-ideal behavior of Fe-FeS liquidus on the iron-rich side of the Fe-FeS phase diagram. In this parametrization, the excess contribution to the Gibbs energy is linear in temperature. As a consequence, the thermal expansivity and isobaric heat capacity of the solution depend only on the end-members.

The ideal and excess thermoelastic properties of the solution are obtained from its Gibbs energy (e.g., Poirier et al. 2000), and the Grüneisen parameter required for calculating the sound velocity (Eq. 8) is computed from

$$\gamma = \left(\frac{C_P}{\alpha K_T V} - \alpha T \right)^{-1} \quad (9)$$

where α, K_T, V, and C_P are the thermal expansivity, isothermal bulk-modulus, volume, and isobaric heat capacity of the solution.

Ideal mixing

The ideal mixing volume between the two end-members is described by the following equation:

$$V = (1-x)V_{Fe} + xV_{FeS} \quad (10)$$

where V is the volume of the considered liquid alloy, x the mole fraction of FeS, and V_{Fe} the volume of liquid Fe and V_{FeS} the volume of liquid FeS.

Such a simple model cannot reproduce our density data set (Fig. 10). The density calculated from Equation 10 decreases too rapidly with increasing S concentration and does not reproduce the positive curvature of density as a function of S content seen in the data (Fig. 10).

Pressure-independent volume Margules parameters

In this non-ideal mixing model, the volume is:

$$V = (1-x)V_{Fe} + xV_{FeS} + (1-x)x[W_{V,Fe}(1-x) + W_{V,FeS}x] \quad (11)$$

where $W_{V,Fe}$ and $W_{V,FeS}$ are the volume Margules parameters. The values of those parameters have been estimated by fitting Equation 11 on the density data (case A) and on the sound velocity data (case B) separately (Table 3).

The density data are well described in case A, but the predicted sound velocities do not agree with the measurements. Conversely, a fit to the sound velocity data provides a good representation of the sound velocity (case B) but fails to describe the experimental density data. This simple Margules mixing model is well suited for modeling the Fe-rich side of the Fe-S phase diagram and the density of Fe-S solutions, however, as shown in case B, a different non-ideal behavior is required to describe the sound velocity data. With Equation 11, the sound velocity is only affected by the non-ideality through the volume but not through the bulk modulus. A non-ideal contribution to the bulk modulus requires that the volume Margules coefficients depend on pressure, as discussed in the next section.

Pressure-dependent volume Margules parameters

By trial and error, we have found that the density and sound velocity data can be well described if we adopt the following parametrization for the volume Margules parameters:

$$W_{V,Fe} = W_{11} + W_{12} \ln\left(\frac{3}{2} + P\right) \quad (12)$$

$$W_{V,FeS} = W_{21} + W_{22}P. \quad (13)$$

TABLE 2. Parameters for liquid FeS equation of state following Vinet and Anderson-Gruneisen parameterization (see Komabayashi 2014 more details)

Reference temperature T_0 (K)	1650
Reference volume (after Nagamori corrected for T = 1650 K) (cm³/mol)	11.8
Reference thermal expansion (after Kaiura) (K^{-1})	1.29E-04
K_{T0} (GPa)	16.5 (0.5)
K'_{T0}	6.21
Υ	1
Q	0

TABLE 3. Margules parameters for pressure-independent and pressure-dependent parameterization

	Model A	Model B
$W_{V,Fe}$	–6.74 ± 0.63	4.93 ± 0.92
$W_{V,FeS}$	–0.47 ± 0.51	5.70 ± 0.87
	P-dependent model	
W11	–7.78 ± 0.95	
W12	2.31 ± 0.14	
W21	–2.32 ± 0.88	
W22	0.057 ± 0.024	

Note: These parameters are given cm³/mol.

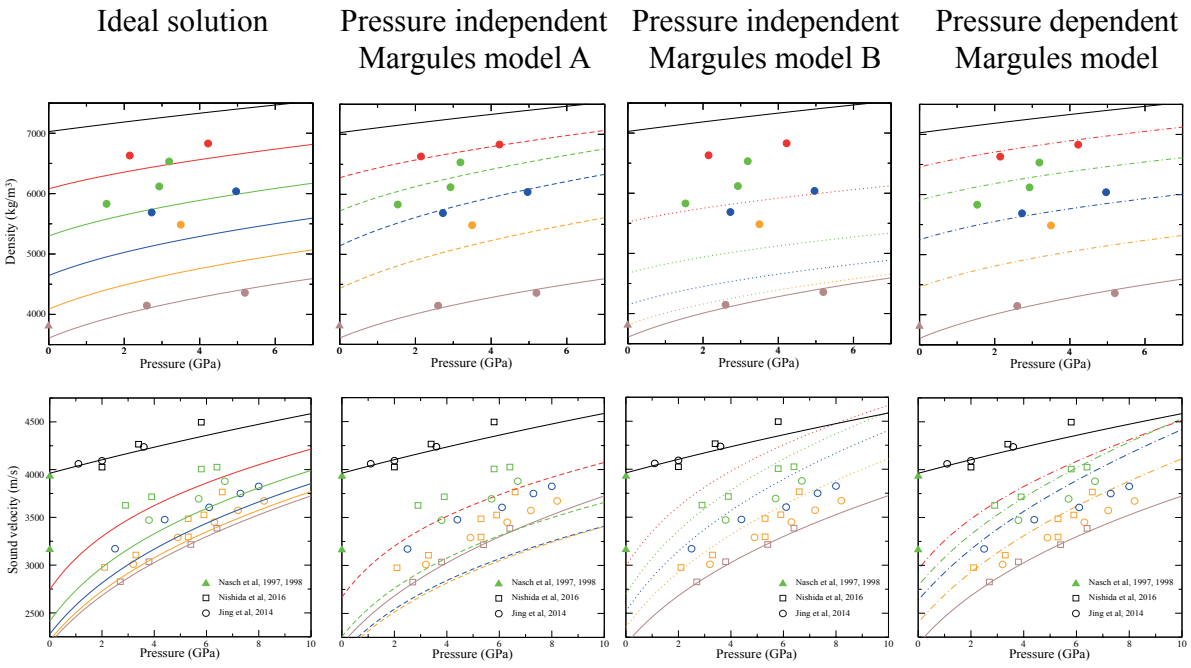

FIGURE 10. Thermodynamic models of density and sound velocity of liquid Fe-S alloys at 1900 K. Four different models have been tested: ideal solution, pressure-independent (Models A and B), and pressure-dependent Margules parameters. It is clear that the pressure dependence of the Margules parameters is required to represent adequately the experimental values. (Color online.)

The estimated values for the parameters W are given in Table 3. They have been obtained by fitting the equations describing the volume and sound velocity on the density and sound velocity data at the same time. As can be seen from Figure 10, this parameterization for the liquid solution gives an adequate description of the experimental data in the 0–8 GPa pressure range. Note that this parametrization cannot be used to model thermoelastic properties beyond that pressure range because an already moderate extrapolation in pressure would lead to unphysical properties.

IMPLICATIONS

To infer the size and sulfur content of planetary cores from seismic or geodesy data requires an accurate knowledge of density and velocity properties of solid and liquid iron alloys as a function of pressure, temperature, and sulfur content. Until now, no consensus on experimental measurements on Fe-S liquid alloys has been reached, with strong contradictions between the different high-pressure studies, and also large disagreement with ambient pressure data. In the present work, we presented new experimental density data of liquid Fe-S alloys at high pressure and high temperature, together with ab initio liquid structure calculations. Combining this new data set and literature data, we were able to establish an empirical and a thermodynamic model for liquid Fe-S solutions that allow computing thermoelastic properties of the liquid alloy as a function of pressure, temperature, and sulfur concentration.

To illustrate the effect of the new density data on the internal structure of small planets, we compare the composition of the Moon's core predicted by our empirical and thermodynamic Fe-S mixing model with a core model assuming ideal mixing between liquid iron and liquid Fe-10wt%S (Fig. 11). The thermoelastic properties of the core in the ideal mixing model are calculated following Dumberry and Rivoldini (2015) and are based on the EoS of liquid Fe (Komabayashi 2014) and Fe-10wt%S (Balog et al. 2003). The aim of this model is to emphasize that liquid

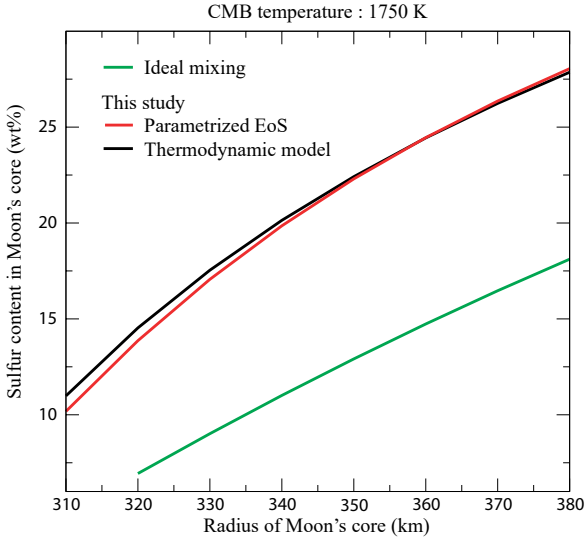

FIGURE 11. The radius of Moon's core as a function of S content of an entirely liquid core, using models presented in this study (parametrized EoS and thermodynamic model) compared with an ideal solution based on previous density measurements (Balog et al. 2003). Calculations were performed for a temperature at the Moon CMB of 1750 K. (Color online.)

Fe-S alloys EoS directly affect the Moon's core composition deduced from its radius.

For our global Moon model, we use the density profile of the silicate part of the Moon structure deduced by Weber et al. (2011) from seismic data, the core models listed in the previous paragraph, and assume that the entire core is in the liquid state, convecting and composed of iron and sulfur. To agree with the most recent moment of inertia estimate (Williams et al. 2014), we had to reduce the density of the upper part of the mantle by about 0.1%. The pressure in the planet is calculated by solving the hydrostatic pressure equation and Poisson equation. The temperature profile in the core is obtained by integrating the adiabatic gradient equation in the core (e.g., Dumberry and Rivoldini 2015) assuming a core-mantle boundary (CMB) temperature of 1750 K. All thermoelastic properties of the core are calculated from the mixing models as a function of pressure, temperature, and composition.

Our results show that for a given core radius, models based on the new elastic data require approximately twice the amount of sulfur than models based on an equation of state deduced from previous elastic data (Fig. 11). Of note, the sulfur concentrations required by the empirical and the thermodynamic model are very similar, even when the two models are based on different sets of acoustic velocity data. Models that agree at 1σ with the moment of inertia have a core radius below about 360 km, but the specifics of the core model have only a very negligible effect on the moment inertia of the planet. However, the larger amount of sulfur required by the new elastic data significantly affects the thermal evolution of the core (i.e., the liquidus of the core decreases with increasing S content) and with it the dynamo action, by delaying the onset of crystallization of iron-rich compounds in the core. The present model assumes a specific CMB temperature (1750 K) that is expected in the present-day core of the Moon (Laneuville et al. 2014). Lowering the CMB temperature will somewhat increase the sulfur content required for the core to match the mass constraint and initiate the crystallization of iron-rich compounds close to the CMB, because the core isentrope is likely steeper than the liquidus (Williams 2009; Breuer et al. 2015). Irrespectively of the assumptions, the present model is a clear illustration of the impact of our two models on Moon's core composition.

The present study, anchored on experimental measurements and theoretical calculations, allows for a coherent model for planetary cores, with applications ranging from the direct simulations of small planetary cores dynamics to the inversion of seismic data (Garcia et al. 2011; Weber et al. 2011; Antonangeli et al. 2015).

ACKNOWLEDGMENTS

The authors thank Stany Bauchau (ESRF) for his help with the X-ray experiments. This work was supported by the Planetlab program of the French National Research Agency (ANR), grant No. ANR-12-BS04-001504. A.R. is supported by the Belgian PRODEX program managed by the European Space Agency in collaboration with the Belgian Federal Science Policy Office

REFERENCES CITED

Alfè, D., and Gillan, M.J. (1998) First-principles simulations of liquid Fe-S under Earth's core conditions. Physical Review B, 58, 8248–8256.

Andrault, D., Bolfan-Casanova, N., Ohtaka, O., Fukui, H., Arima, H., Fialin, M., and Funakoshi, K. (2009) Melting diagrams of Fe-rich alloys determined from synchrotron in situ measurements in the 15–23 GPa pressure range. Physics of the Earth and Planetary Interiors, 174, 181–191.

Antonangeli, D., Morard, G., Schmerr, N.C., Komabayashi, T., Krisch, M., Fiquet, G., Fei, Y., and Mao, H.-K. (2015) Toward a mineral physics reference model for the Moon's core. Proceedings of the National Academy of Sciences, 112.

Assael, M.J., Kakosimos, K., Banish, R.M., Brillo, J., Egry, I., Brooks, R., Quested, P.N., Mills, K.C., Nagashima, A., Sato, Y., and others. (2006) Reference data for the density and viscosity of liquid aluminum and liquid iron. Journal of Physical and Chemical Reference Data, 35, 285–300.

Balog, P.S., Secco, R.A., Rubie, D.C., and Frost, D.J. (2003) Equation of state of liquid Fe^{-10} wt% S: Implications for the metallic cores of planetary bodies. Journal of Geophysical Research-Solid Earth, 108.

Besson, J.M., Nelmes, R.J., Hamel, G., Loveday, J.S., Weill, G., and Hull, S. (1992) Neutron diffraction above 10 GPa. Physica B: Condensed Matter, 181, 907–910.

Blochl, P.E. (1994) Projector augmented-wave method. Physical Review B, 50.

Bottin, F., Leroux, S., Knyazev, A., and Zérah, G. (2008) Large-scale ab initio calculations based on three levels of parallelization. Computational Materials Science, 42, 329–336.

Bouchet, J., Mazevet, S., Morard, G., Guyot, F., and Musella, R. (2013) Ab initio equation of state of iron up to 1500 GPa. Physical Review B—Condensed Matter and Materials Physics, 87, 1–8.

Breuer, D., Rueckriemen, T., and Spohn, T. (2015) Iron snow, crystal floats, and inner-core growth: modes of core solidification and implications for dynamos in terrestrial planets and moons. Progress in Earth and Planetary Science, 2, 1–26.

Buono, A.S., and Walker, D. (2011) The Fe-rich liquidus in the Fe-FeS system from 1bar to 10GPa. Geochimica et Cosmochimica Acta, 75, 2072–2087.

Campbell, A.J., Seagle, C.T., Heinz, D.L., Shen, G., and Prakapenka, V.B. (2007) Partial melting in the iron-sulfur system at high pressure: A synchrotron X-ray diffraction study. Physics of the Earth and Planetary Interiors, 162, 119–128.

Chabot, N.L. (2004) Sulfur contents of the parental metallic cores of magmatic iron meteorites. Geochimica et Cosmochimica Acta, 68, 3607–3618.

Chen, B., Gao, L., Leinenweber, K., Wang, Y., Sanehira, T., and Li, J. (2008a) In situ investigation of high-pressure melting behavior in the Fe-S system using synchrotron X-ray radiography. High Pressure Research, 28, 315–326.

Chen, B., Li, J., and Hauck, S.A. (2008b) Non-ideal liquidus curve in the Fe-S system and Mercury's snowing core. Geophysical Research Letters, 35, 10–14.

Chen, B., Li, Z., Zhang, D., Liu, J., Hu, M.Y., Zhao, J., Bi, W., Alp, E.E., Xiao, Y., Chow, P., and others. (2014) Hidden carbon in Earth's inner core revealed by shear softening in dense Fe_7C_3. Proceedings of the National Academy of Sciences, 111, 17755–17758.

Chen, J., Yu, T., Huang, S., Girard, J., and Liu, X. (2014) Compressibility of liquid FeS measured using X-ray radiograph imaging. Physics of the Earth and Planetary Interiors, 228, 294–299.

Chudinovskikh, L., and Boehler, R. (2007) Eutectic melting in the system Fe-S to 44 GPa. Earth and Planetary Science Letters, 257, 97–103.

Dewaele, A., Torrent, M., Loubeyre, P., and Mezouar, M. (2008) Compression curves of transition metals in the Mbar range: Experiments and projector augmented-wave calculations. Physical Review B—Condensed Matter and Materials Physics, 78, 1–13.

Dumberry, M., and Rivoldini, A. (2015) Mercury's inner core size and core-crystallization regime. ICARUS, 248, 254–268.

Flory, M.A., McLamarrah, S.K., and Ziurys, L.M. (2005) High-resolution spectroscopy of CoS ($X^4\Delta_i$): Examining 3*d* transition-metal sulfide bonds. Journal of Chemical Physics, 123, 1–9.

Garcia, R.F., Gagnepain-Beyneix, J., Chevrot, S., and Lognonné, P. (2011) Very preliminary reference Moon model. Physics of the Earth and Planetary Interiors, 188, 96–113.

Gonze, X., Jollet, F., Abreu Araujo, F., Adams, D., Amadon, B., Applencourt, T., Audouze, C., Beuken, J.M., Bieder, J., Bokhanchuk, A., and others. (2016) Recent developments in the ABINIT software package. Computer Physics Communications, 205, 106–131.

Greenwood, R.C., Franchi, I.A., Jambon, A., Barrat, J.A., and Burbine, T.H. (2006) Oxygen isotope variation in stony-iron meteorites. Science, 313, 1763.

Hammersley, A.P., Svensson, S.O., Hanfland, M., Fitch, A.N., and Hausermann, D. (1996) Two-dimensionnal detector software: from real detector to idealised image or two-theta scan. High Pressure Research, 14, 235–248.

Jing, Z., Wang, Y., Kono, Y., Yu, T., Sakamaki, T., Park, C., Rivers, M.L., Sutton, S.R., and Shen, G. (2014) Sound velocity of Fe-S liquids at high pressure: Implications for the Moon's molten outer core. Earth and Planetary Science Letters, 396, 78–87.

Kaiura, G.H., and Toguri, J.M. (1979) Densities of the molten FeS, FeS-Cu_2S and Fe-S-O systems—utilizing a bottom-balance Archimedean technique. Canadian Metallurgical Quarterly, 18, 155–164.

Kamada, S., Ohtani, E., Terasaki, H., Sakai, T., Miyahara, M., Ohishi, Y., and Hirao, N. (2012) Melting relationships in the Fe-Fe^3S system up to the outer core conditions. Earth and Planetary Science Letters, 359-360, 26–33.

Kleine, T., Touboul, M., Bourdon, B., Nimmo, F., Mezger, K., Palme, H., Jacobsen, S.B., Yin, Q., and Halliday, A.N. (2009) Hf–W chronology of the accretion and early evolution of asteroids and terrestrial planets. Geochimica et Cos-

mochimica Acta, 73, 5150–5188.
Klotz, S., Strässle, T., Rousse, G., Hamel, G., and Pomjakushin, V. (2005) Angle-dispersive neutron diffraction under high pressure to 10 GPa. Applied Physics Letters, 86, 1–3.
Klotz, S., Le Godec, Y., Strässle, T., and Stuhr, U. (2008) The α-γ-ε triple point of iron investigated by high pressure-high temperature neutron scattering. Applied Physics Letters, 93, 2008–2010. doi:10.1063/1.2976128
Komabayashi, T. (2014) Thermodynamics of melting relations in the system Fe-FeO at high pressure: Implications for oxygen in the Earth's core. Journal of Geophysical Research: Solid Earth, 119, 4164–4177.
Kono, Y., Kenney-Benson, C., Shibazaki, Y., Park, C., Shen, G., and Wang, Y. (2015) High-pressure viscosity of liquid Fe and FeS revisited by falling sphere viscometry using ultrafast X-ray imaging. Physics of the Earth and Planetary Interiors, 241, 57–64.
Kuskov, O.L., and Belashchenko, D.K. (2016) Thermodynamic properties of Fe-S alloys from molecular dynamics modeling: Implications for the lunar fluid core. Physics of the Earth and Planetary Interiors, 258, 43–50.
Laneuville, M., Wieczorek, M.A., Breuer, D., Aubert, J., Morard, G., and Rückriemen, T. (2014) A long-lived lunar dynamo powered by core crystallization. Earth and Planetary Science Letters, 401.
LeBlanc, G.E., and Secco, R.A. (1996) Viscosity of an Fe-S liquid up to 1300 degrees C and 5 GPa. Geophysical Research Letters, 23, 213–216.
Margot, J.L., Peale, S.J., Jurgens, R.F., Slade, M.A., and Holin, I.V (2007) Large longitude libration of Mercury reveals a molten core. Science, 316, 710–714.
Mezouar, M., Le Bihan, T., Libotte, H., Le Godec, Y., and Häusermann, D. (1999) Paris-Edinburgh large-volume cell coupled with a fast imaging plate system for structural investigation at high pressure and high-temperature. Journal of Synchrotron Radiation, 6, 1115–1119.
Mezouar, M., Faure, P., Crichton, W., Rambert, N., Sitaud, B., Bauchau, S., and Blattmann, G. (2002) Multichannel collimator for structural investigation of liquids and amorphous materials at high pressures and temperatures. Review of Scientific Instruments, 73, 3570.
Mezouar, M., Crichton, W.A., Bauchau, S., Thurel, F., Witsch, H., Torrecillas, F., Blattman, G., Marion, P., Dabin, Y., Chavanne, J., and others. (2005) Development of a new state-of-the-art beamline optimized for monochromatic single crystal and powder X-ray diffraction under extreme conditions at the ESRF. Journal of Synchrotron Radiation, 12, 659–664.
Morard, G., Mezouar, M., Rey, N., Poloni, R., Merlen, A., Le Floch, S., Toulemonde, P., Pascarelli, S., San-Miguel, A., Sanloup, C., and others. (2007a) Optimization of Paris-Edinburgh press cell assemblies for in situ monochromatic X-ray diffraction and X-ray absorption. High Pressure Research, 27, 223–233.
Morard, G., Sanloup, C., Fiquet, G., Mezouar, M., Rey, N., Poloni, R., and Beck, P. (2007b) Structure of eutectic Fe-FeS melts to pressures up to 17 GPa: Implications for planetary cores. Earth and Planetary Science Letters, 263, 128–139.
Morard, G., Andrault, D., Guignot, N., Sanloup, C., Mezouar, M., Petitgirard, S., and Fiquet, G. (2008a) In situ determination of Fe-Fe_3S phase diagram and liquid structural properties up to 65 GPa. Earth and Planetary Science Letters, 272, 620–626.
Morard, G., Sanloup, C., Guillot, B., Fiquet, G., Mezouar, M., Perrillat, J.P., Garbarino, G., Mibe, K., Komabayashi, T., and Funakoshi, K. (2008b) In situ structural investigation of Fe-S-Si immiscible liquid system and evolution of Fe-S bond properties with pressure. Journal of Geophysical Research: Solid Earth, 113, 1–12.
Morard, G., Mezouar, M., Bauchau, S., Lvarez-Murga, M., Hodeau, J.L., and Garbarino, G. (2011) High efficiency multichannel collimator for structural studies of liquids and low-Z materials at high pressures and temperatures. Review of Scientific Instruments, 82, 2–7.
Morard, G., Siebert, J., Andrault, D., Guignot, N., Garbarino, G., Guyot, F., and Antonangeli, D. (2013) The Earth's core composition from high pressure density measurements of liquid iron alloys. Earth and Planetary Science Letters, 373.
Nagamori, M. (1969) Density of molten Ag–S, Cu–S, Fe–S, and Ni–S systems. Transactions of the Metallurgical Society AIME, 245, 1897–1902.
Nasch, P.M., and Manghnani, M.H. (1998) Molar volume, thermal expansion, and bulk modulus in liquid Fe-Ni alloys at 1 bar: Evidence for magnetic anomalies? Geophysical Monograph, 101, 307–317.
Nasch, P.M., and Steinemann, S.G. (1995) Density and thermal expansion of molten manganese, iron, nickel, copper, aluminum and tin by means of the gamma-ray attenuation technique. Physics and Chemistry of Liquids, 29, 43–58.
Nasch, P., Manghnani, M., and Secco, R. (1997) Anomalous behavior of sound velocity and attenuation in liquid Fe-Ni-S. Science, 277, 219.
Nishida, K., Terasaki, H., Ohtani, E., and Suzuki, A. (2008) The effect of sulfur content on density of the liquid Fe-S at high pressure. Physics and Chemistry of Minerals, 35, 417–423.
Nishida, K., Ohtani, E., Urakawa, S., Suzuki, A., Sakamaki, T., Terasaki, H., and Katayama, Y. (2011) Density measurements of liquid FeS at high pressures using synchrotron X-ray absorption. American Mineralogist, 96, 864–868.
Nishida, K., Kono, Y., Terasaki, H., Takahashi, S., Ishii, M., Shimoyama, Y., Higo, Y., Funakoshi, K.I., Irifune, T., and Ohtani, E. (2013) Sound velocity measurements in liquid Fe-S at high pressure: Implications for Earth's and lunar cores. Earth and Planetary Science Letters, 362, 182–186.
Nishida, K., Suzuki, A., Terasaki, H., Shibazaki, Y., Higo, Y., Kuwabara, S., Shimoyama, Y., Sakurai, M., Ushioda, M., Takahashi, E., and others. (2016) Towards a consensus on the pressure and composition dependence of sound velocity in the liquid Fe–S system. Physics of the Earth and Planetary Interiors, 257, 230–239.
Perdew, J.P., Burke, K., and Ernzerhof, M. (1996) Generalized gradient approximation made simple. Physical Review Letters, 77, 3865–3868.
Poirier, J.P. (1994) Light elements in the Earth's outer core: A critical review. Physics of the Earth and Planetary Interiors, 85, 319–337.
——— (2000) Introduction to the Physics of the Earth's Interior. Cambridge University Press.
Pourovskii, L.V., Miyake, T., Simak, S.I., Ruban, A.V., Dubrovinsky, L., and Abrikosov, I.A. (2013) Electronic properties and magnetism of iron at the Earth's inner core conditions. Physical Review B—Condensed Matter and Materials Physics, 87.
Rivoldini, A., Van Hoolst, T., and Verhoeven, O. (2009) The interior structure of Mercury and its core sulfur content. Icarus, 201, 12–30.
Sanloup, C., Guyot, F., Gillet, P., Fiquet, G., Mezouar, M., and Martinez, I. (2000) Density measurements of liquid Fe-S alloys at high pressure. Geophysical Research Letters, 27, 811–814.
Sherman, D.M. (1995) pressure and the composition of the Earth's core. Earth and Planetary Science Letters, 132, 87–98.
Stewart, A.J., Schmidt, M.W., van Westrenen, W., and Liebske, C. (2007) Mars: A New Core-Crystallization Regime. Science, 316, 1323–1325.
Torrent, M., Jollet, F., Bottin, F., Zérah, G., and Gonze, X. (2008) Implementation of the projector augmented-wave method in the ABINIT code: Application to the study of iron under pressure. Computational Materials Science, 42, 337–351.
Tsuchiya, Y. (1994) The thermodynamics of structural changes in the liquid sulphur-tellurium system: compressibility and Ehrenfest's relations. Journal of Physics: Condensed Matter, 6, 2451.
Urakawa, S., Someya, K., Terasaki, H., Katsura, T., Yokoshi, S., Funakoshi, K.-i., Utsumi, W., Katayama, Y., Sueda, Y.-i., and Irifune, T. (2004) Phase relationships and equations of state for FeS at high pressures temperatures and implications for the internal structure of Mars. Physics of the Earth and Planetary Interiors, 143, 469–479. doi:10.1016/j.pepi.2003.12.015
Utsumi, W., Weidner, D.J., and Liebermann, R.C. (1998) Volume measurement of MgO at high pressures and high temperatures. Geophysical Monograph, 101, 327–333.
Vočadlo, L., Alfè, D., Price, G.D., and Gillan, M.J. (2000) First principles calculations on the diffusivity and viscosity of liquid Fe-S at experimentally accessible conditions. Physics of the Earth and Planetary Interiors, 120, 145–152.
Weber, R.C., Lin, P.-Y., Garnero, E.J., Williams, Q., and Lognonne, P. (2011) Seismic Detection of the lunar Core. Science, 331, 309–312.
Williams, Q. (2009) Bottom-up versus top-down solidification of the cores of small solar system bodies: Constraints on paradoxical cores. Earth and Planetary Science Letters, 284, 564–569.
Williams, J.G., Konopliv, A.S., Boggs, D.H., Park, R.S., Yuan, D., Lemoine, F.G., Goossens, S., Mazarico, E., Nimmo, F., Weber, R.C., and others. (2014) lunar interior properties from the GRAIL mission. Journal of Geophysical Research: Planets, 119, 1546–1578.
Yoder, C.F., Konopliv, A.S., Yuan, D.N., Standish, E.M., and Folkner, W.M. (2003) Fluid core size of Mars from detection of the solar tide. Science, 300, 299–303.
Yoshino, T., Walter, M.J., and Katsura, T. (2003) Core formation in planetesimals triggered by permeable flow. Nature, 422, 154–157.
Zhang, Z., and Pommier, A. (2017) Electrical investigation of metal-olivine systems and application to the deep interior of Mercury. Journal of Geophysical Research: Planets, 122, 2702–2718.

Manuscript received November 23, 2017
Manuscript accepted July 6, 2018
Manuscript handled by Heather Watson